Eur. Phys. J. A (2026) 62:25
https://doi.org/10.1140/epja/s10050-025-01769-1

THE EUROPEAN PHYSICAL JOURNAL A

Regular Article - Experimental Physics

The Advanced Plunger-Particle detector Array - APPA

E. Uusikylä [1,a], P. Ruotsalainen [1], T. Grahn [1], C. Müller-Gatermann [2], C. Fransen [3], S. Thiel [3], M. Beckers [3], A. Illana [1,6], C.-D. Lakenbrink [3], D. Lazzaretto [1], J. Sarén [1], K. Auranen [1], V. Bogdanoff [1], A. D. Briscoe [1,4], L. Canete [5], J. Chadderton [4], P. Greenlees [1], J. Heery [5], A. Javanainen [1,11], J. Jolie [3], H. Joukainen [1], R. Julin [1], H. Jutila [1], H. Kokkonen [1], J. Louko [1], M. Luoma [1,12], A. M. Plaza [1,4], B. S. Nara Singh [7], J. Ojala [1], J. Pakarinen [1], P. Rahkila [1], J. Romero [1], S. Suman [8], J. Tuunanen [1], J. Uusitalo [1], F. von Spee [3,9], G. L. Zimba [1,10]

[1] Accelerator Laboratory, Department of Physics, University of Jyväskylä, 40014 Jyväskylä, Finland
[2] Physics Division, Argonne National Laboratory, Lemont, IL 60439, USA
[3] Institut für Kernphysik, Universität zu Köln, 50937 Köln, Germany
[4] Department of Physics, Oliver Lodge Laboratory, University of Liverpool, Liverpool L69 7ZE, UK
[5] School of Mathematics and Physics, University of Surrey, Guildford GU2 7XH, UK
[6] Grupo de Física Nuclear & IPARCOS, 28040 Madrid, Spain
[7] School of Computing Engineering and Physical Sciences, CEI Moncloa, Universidad Complutense de Madrid, 28040 Madrid, Spain
[8] Department of Physics "E. Pancini", University of Naples Federico II, 80126 Naples, Italy
[9] Ir'ene Joliot-Curie Laboratory, CNRS/IN2P3, 91405 Orsay, France
[10] Facility for Rare Isotope Beams, Michigan State University, 640 South Shaw Lane, East Lansing, MI 48824, USA
[11] Department of Electrical and Computer Engineering, Vanderbilt University, Nashville 37235, USA
[12] Helsinki Institute of Physics, University of Helsinki, Helsinki 00014, Finland

Received: 15 August 2025 / Accepted: 8 December 2025

Communicated by Wolfram Korten

Abstract The Advanced Plunger-Particle detector Array (APPA) is a new plunger device constructed to measure lifetimes of excited states in exotic nuclei, particularly those near the $N = Z$ line. This instrument combines a compact plunger device with a charged-particle detector array to increase the experimental sensitivity for low-cross-section lifetime measurements employing fusion-evaporation reactions. APPA can be used in conjunction with the JUROGAM 3 germanium-detector array and with the RITU or MARA recoil separators available at the Accelerator Laboratory of the University of Jyväskylä (JYFL-ACCLAB). This article outlines the technical details of APPA, presents the lifetime measurement of the 2_1^+ state in ^{62}Zn, and reports the effect of APPA on the transmission efficiency of MARA and prompt γ-ray and JYUTUBE detection efficiencies.

1 Introduction

The measurement of nuclear transition strengths provides a wealth of information about nuclear structure. Strength of the electric quadrupole $E2$ transitions between the excited states of a nucleus is closely related to the degree of collective motion of the nucleons manifested in nuclear charge distributions that deviate from sphericity or the vibration of spherical systems. The study of the development of nuclear collectivity and shape evolution deepens our understanding of the properties of the strong nuclear force. For example, the region of nuclei with $A = 56$–100 around the $N = Z$ line between doubly-closed shells is known to exhibit a remarkable diversity of nuclear shapes (see, e.g., Refs. [1–3]). In this region, nuclear shapes evolve as a function of the mass number from spherical to triaxial, oblate, prolate, and back to spherical. This evolution is induced by the occupation of deformation-driving single-particle orbitals. Moreover, the coexistence of different nuclear shapes has been observed in several nuclei, such as in the recently studied ^{190}Pb isotope [4–6].

The reduced transition strengths (the B($E2$) values from now on) can be determined from the lifetimes of the excited states. When combining measurements of the B($E2$) values with Coulomb excitation data, spectroscopic quadrupole moments Q_s can be extracted (see, e.g., [7]). The B($E2$) and Q_s values are the most significant measures of quadrupole collectivity and nuclear shape, respectively. Lifetimes of excited states in the 10^{-12}–10^{-9} s regime can be measured

[a] e-mail: eetu.j.e.uusikyla@jyu.fi (corresponding author)

Published online: 03 February 2026

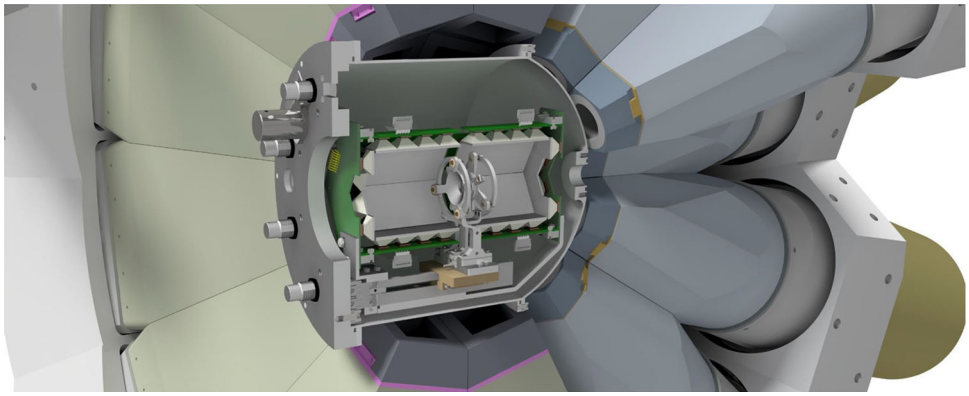

Fig. 1 Side profile of APPA inside the JUROGAM 3 target chamber. The ion beam enters from the right. Nuclei of interest are synthesized in the target foil and pass through the degrader foil towards the recoil separator

using the Recoil Distance Doppler-Shift (RDDS) method [8], employing, e.g., fusion-evaporation reactions.

A decade ago, the heaviest odd-odd $N = Z$ nucleus, for which a $B(E2; 2^+ \rightarrow 0^+)$ value had been measured, was ^{58}Cu [9]. The situation has improved since the $B(E2; 2^+ \rightarrow 0^+)$ values in ^{70}Br, ^{74}Rb, and ^{78}Y have been reported in Refs. [2,3,10,11], in addition to the data on ^{46}V and ^{50}Mn [12–14]. The odd-odd $N = Z$ nuclei in the A = 18–78 region for which the $B(E2; 2^+ \rightarrow 0^+)$ values have not yet been measured are ^{54}Co, ^{62}Ga and ^{66}As. The level schemes of the ^{62}Ga and ^{66}As nuclei have recently been studied with the Recoil-Beta-Tagging (RBT) technique at the Accelerator Laboratory of the Department of Physics (JYFL-ACCLAB) [15–17]. The Advanced Plunger-Particle detector Array (APPA), developed at the Institute of Nuclear Physics, Cologne, Germany, was born from the idea of combining the plunger lifetime measurement method with the RBT technique to access the lifetimes in these exotic nuclei. As previous in-beam γ-ray spectroscopy studies around the $N = Z$ line employing the RBT technique have shown, the use of a charged-particle veto detector is highly beneficial [16,18,19]. Consequently, combining a plunger device with a charged-particle detector array increases the experimental sensitivity in lifetime measurements of weakly populated nuclear excited states. This, however, requires a compact size for the plunger device. Instruments employing both a plunger and a charged-particle detector have also been developed in other research facilities around the world, for example, the Tigress Integrated Plunger (TIP) used at TRIUMF [20], the GALILEO plunger developed for Laboratori Nazionali di Legnaro [21], iCAPS (integrated Cologne Argonne Plunger Setup) used at the ATLAS facility at Argonne National Laboratory (ANL) [22], and reversed plunger used together with the AGATA array [23].

2 Materials and methods

2.1 Mechanical design of APPA

The APPA instrument, shown in Fig. 1, combines a compact plunger device with the JYUTUBE (Jyväskylä–York University Tube) charged-particle detector array. It is placed in the center of the target chamber, which is surrounded by the JUROGAM 3 germanium-detector array [24] as shown in Fig. 1. The design drawing of the APPA plunger is shown in Fig. 2. The plunger is a device for lifetime measurements employed with the recoil distance Doppler-shift (RDDS) technique. It includes parallel, conductive target and degrader foils. Using the degrader foil instead of the conventional stopper foil allows the fusion-evaporation reaction products to enter a recoil separator. The foils are glued to aluminum frames (1. in Fig. 2). Each foil is stretched over the aluminum-target and degrader cones (2. and 3. in Fig. 2) with circular openings of 8 and 10 mm, respectively, by three spring-loaded screws (4. in Fig. 2). The resulting flat foil surfaces are aligned to be parallel with respect to each other by visually observing light through the gap between the foils. The alignment is adjusted via three spring-loaded screws (5. in Fig. 2) that attach the target cone to its support ring (6. in Fig. 2), while the degrader cone is directly mounted on its support ring. The support rings are attached to the target and degrader stands (7. and 8. in Fig. 2). The target stand is attached to the Q−521.140 Miniature Linear Stage [25] (9. in Fig. 2), manufactured by the company Physik Instrumente (PI). For simplification, in the following the Q−521.140 Linear Stage is referred as ”motor”. The motor has a travel range of 12 mm, a position sensor resolution of 1 nm, and a minimum incremental motion of 30 nm. The degrader stand is mounted to the fixed electrically insulating base structure (10. in Fig. 2). The APPA plunger can be laterally aligned with the ion optical axis of the beam from the base structure (11. in Fig. 2).

The APPA plunger was constructed specifically for use with JYUTUBE. The main design criterion was to minimize the shadowing of the JYUTUBE detector elements by the plunger structures, and therefore the motor is also placed outside of JYUTUBE. Secondly, this design was to minimize the possible electromagnetic interference between the motor and the JYUTUBE detectors. Such interference has not been observed in the JYUTUBE detector signals.

2.2 Distance calibration and measurement

For lifetime measurements with the RDDS technique employing a plunger device, the target-to-degrader distance is varied. In the APPA plunger, the distance is adjusted by moving the target stand with the motor. The distance based on the number and size of the motor steps taken is called **motor distance**. This is the relative distance from the **zero-point position**, which is defined by the user. The absolute distance between the foils cannot be directly extracted from the motor distance. Instead, a capacitance method, as outlined in Ref. [26], is used. The block diagram for the distance measurement is shown in Fig. 3. A flat-top voltage pulse with an amplitude V_0 from the Model PB-5 Pulse Generator [27], manufactured by BNC (Berkeley Nucleonics Corporation), is introduced into the target foil. This induces a time-dependent voltage pulse in the degrader foil through capacitive coupling. The induced voltage pulse can be described with $V(t) = V_0 e^{-\frac{t}{RC}}$, where R is the input impedance of the linear amplifier and C is the capacitance between the foils. The time integral of $V(t)$, achieved by the linear amplifier, is linearly proportional to C and thus inversely proportional to the distance between the foils, assuming an ideal plate capacitor. The induced voltage signal is amplified and shaped by the linear amplifier and then digitized to precisely measure its amplitude using the National Instruments NI USB-6212 DAQ device [28].

The relation between induced voltage and motor distance is established in a distance-calibration procedure [26]. First, the electrical contact point must be determined. That point corresponds to the shortest achievable distance before continuous electrical breakdowns occur between the foils. The indication of electrical contact is a sudden increase in the measured voltage due to short circuit between the foils. The motor zero-point position is set to the electrical contact point. After establishing the electrical contact point, the voltage is measured at different motor distances to generate a distance calibration curve, as shown in Fig. 4. An estimate of the absolute minimum distance, called the **offset**, is deduced as explained in the caption of Fig. 4. Further information on this procedure is given in Ref. [29]. The offset in the APPA plunger typically ranges from 5 to 20 μm, depending on the surface quality and alignment of the foils. Determining the offset is not strictly required for the lifetime analysis methods

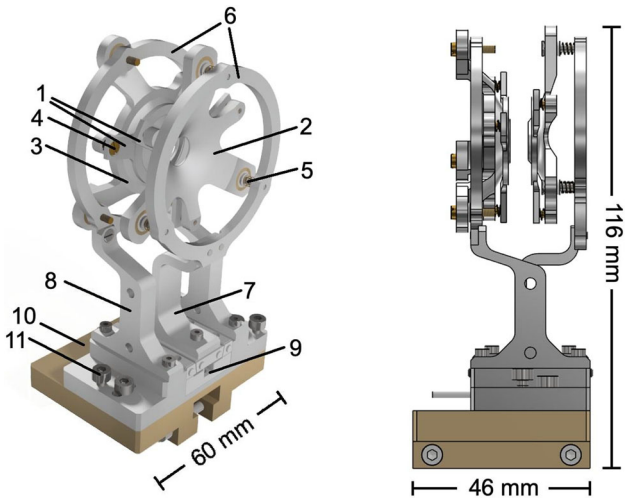

Fig. 2 Isometric view and side projection of the 3D model of the APPA plunger. In the figure on the right, the target is positioned on the right and the degrader on the left. Essential parts of the plunger are assigned in the left-hand side figure as follows: 1. target/degrader frame, 2. target cone, 3. degrader cone, 4. spring-loaded screw for degrader foil stretching, 5. spring-loaded screw for parallel alignment of the foils, 6. target/degrader support ring, 7. target stand, 8. degrader stand, 9. Q−521.140 Linear Stage, 10. electrically insulating base structure and 11. lateral adjustment

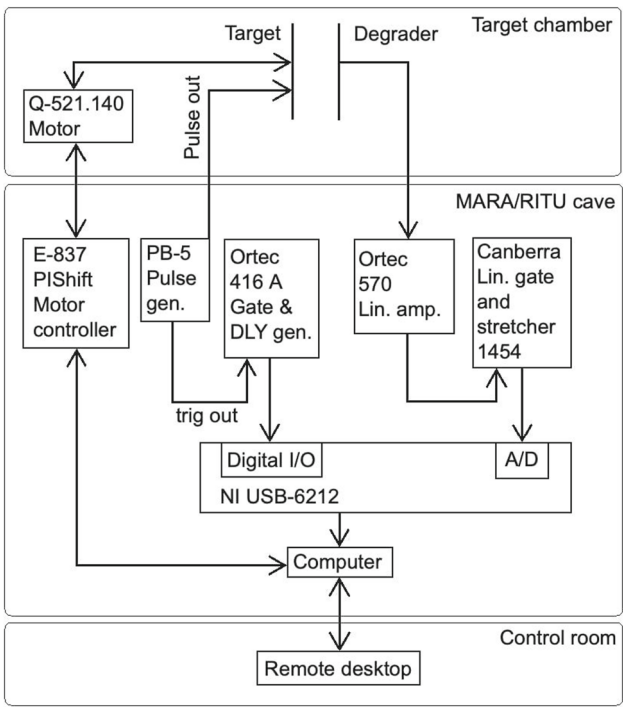

Fig. 3 Block diagram of the target-to-degrader distance measurement and motor control

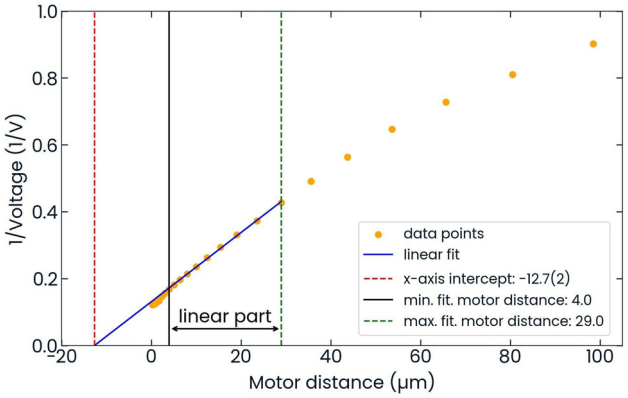

Fig. 4 Distance calibration and estimation of the offset in the case of ^{nat}Mg target and ^{93}Nb degrader. The offset is estimated from the absolute value of the x-axis interception (in this example ∼13 μm, indicated by red dashed line) of the linear fit to the data points. The data points used for the fit are selected based on visual inspection. Moreover, the quoted uncertainty of 0.2 μm for the offset is associated with the linear fit procedure only. A more realistic uncertainty estimate for the offset, as determined with the method used here, is approximately ±5 μm as stated in Ref. [26]. The non-linearity at short distances is due to mechanical contact between the foils and oxide layer on the ^{nat}Mg target, while the non-linearity at longer distances is due to stray capacitance

that are based on relative distances, such as the Differential Decay Curve Method (DDCM) [30] as used in this work. However, it is essential when estimating the lower limit of the measurable lifetime.

When the ion beam impinges on the target foil, the target-to-degrader distance can be affected by momentum transfer [32] in the foils and thermal expansion [31] of the foils and plunger structures, either temporarily or permanently. To compensate for the temporary effects, a LabView-based *Feedback* software has been developed at the Institute for Nuclear Physics of the University of Cologne [29]. The *Feedback* software aims to maintain the capacitance between the two stretched foils and the corresponding foil separation from the distance calibration within the set tolerance limits by automatically adjusting the motor distance—if the measured distance value exceeds the set lower or upper limit, then *Feedback* restores the calibrated distance back within the set distance range. Permanent foil deformations can only be attempted to be corrected by re-stretching the foils. In the case of temporary foil deformations, lowering the beam intensity might help to avoid these problems.

3 APPA commissioning experiment

The APPA commissioning experiment was carried out in JYFL-ACCLAB using a 114-MeV ^{40}Ca beam from the K130 cyclotron [34] to bombard a ^{nat}Mg target with a thickness of 0.74 mg/cm^2. The objectives of the commissioning experiment were to measure *i*) the previously determined lifetime of the 2_1^+ state in ^{62}Zn (see previous results in Table 1), *ii*) the MARA transmission efficiency, *iii*) the MARA mass-resolving power, *iv*) the prompt γ-ray detection efficiency of the JUROGAM 3 spectrometer with the APPA setup in place, and *v*) the JYUTUBE charged-particle detection efficiency in the APPA configuration. In this experiment, ^{62}Zn was produced in the ^{24}Mg(^{40}Ca, 2p)^{62}Zn reaction. For the RDDS lifetime measurement, a ^{93}Nb degrader with a thickness of 1.33 mg/cm^2 was used. The γ-ray intensity is split between the fully Doppler-shifted ($v_{recoil}/c = 0.042(2)$) and degraded components ($v_{recoil}/c = 0.030(4)$), which correspond to γ-rays emitted before and after the degrader foil, respectively.

The vacuum-mode separator MARA [35] was used to separate the recoiling fusion-evaporation reaction products (recoils) with specific mass-to-charge (A/q) ratios from the primary beam particles. At the exit of MARA, the recoils first pass through a Multi-Wire Proportional Counter (MWPC) and are then implanted into a Double-Sided Silicon Strip Detector (DSSD). The DSSD detector was of Micron BB20 type with a thickness of 300 μm. The recoils can be identified by their energy deposited into DSSD and by their time-of-flight between MWPC and DSSD.

The target chamber was surrounded by 13 tapered Compton-suppressed germanium detectors of JUROGAM 3 [24] to detect promptly emitted γ rays. The Ge detectors were arranged in two rings at angles of 157.7° (Ring 1, 4 Ge detectors in the current experiment) and 133.6° (Ring 2, 9 Ge detectors in the current experiment) with respect to the beam direction. Each Ge detector was equipped with a BGO shield for Compton suppression. As part of the APPA device, the charged-particle detector JYUTUBE, consisting of 120 plastic scintillator elements forming a hexagonal barrel, was installed inside the target chamber, surrounding the plunger device, as shown in Fig. 1. JYUTUBE can be used to assist in the selection of the fusion-evaporation channel by measuring the number of evaporated charged particles for each recoil event. All detector signals were fed into 100-MHz Lyrtech/Nutaq VHS-ADC digitizers and recorded in triggerless mode. Data analysis was performed using the Grain software package [36] and the NAPATAU lifetime analysis software [37].

4 Results

4.1 Lifetime measurement

The lifetime measurement of the 2_1^+ state in ^{62}Zn was carried out using the following calibrated target-to-degrader distances with respect to the zero-point position (and measurement times): 15.0(4) μm (t_{meas} = 110 min), 65.0(1) μm

Table 1 Transition energies E_γ and previously measured level lifetimes τ in ^{62}Zn, relevant for the present work

Transition	E_γ (keV)	τ (ps)
$2_1^+ \rightarrow 0_{gs}^+$	953.8(1) [38]	4.2(7) [39]
		4.3(3) [40]
		4.2(3) [41]
		$2.5^{+1.0}_{-2.0}$ [42]
$4_1^+ \rightarrow 2_1^+$	1232.2(1) [38]	$0.76^{+0.34}_{-0.20}$ [41]
		1.5(10) [42]
		1.2(1) [40]

(t_{meas} = 120 min), 105.0(3) μm (t_{meas} = 130 min), 124.0(3) μm (t_{meas} = 114 min), 156.0(4) μm (t_{meas} = 111 min), and 303.0(16) μm (t_{meas} = 310 min). The measurement times were limited to obtain similar statistics as expected for the proposed lifetime measurement of ^{66}As. Moreover, the lifetime analysis was performed separately by employing *i*) recoil- and mass-gated singles γ-ray data and *ii*) stand-alone JUROGAM 3 γ-γ coincidence data.

In DDCM, the lifetime of the state i is extracted using the equation

$$\tau_i(x) = -\frac{I_i^d(x) - \sum_k b_{ki}\alpha_{ki} I_k^d(x)}{v\frac{d}{dx} I_i^S(x)}. \quad (1)$$

Here, I_i^d and I_k^d correspond to the normalized intensities of the degraded components of the specific de-exciting γ-ray transition and each observed feeding γ-ray transitions of the state i, respectively. I_i^S is the normalized intensity of the fully Doppler-shifted component of the de-exciting γ-ray transition. Normalization is performed here based on the ratio $I^{d/S} = \frac{N^{d/S}}{N^d+N^S}$, where N^d and N^S are the fitted peak areas of the degraded and shifted components, respectively. The variable v is the recoil velocity and x is the target-to-degrader distance. The term α_{ki} is given as a relation

$$\alpha_{ki} = \frac{\omega_k(\theta)\cdot\varepsilon(E_{\gamma,k})}{\omega_i(\theta)\cdot\varepsilon(E_{\gamma,i})}, \quad (2)$$

where $\omega(\theta)$ contains the angular distribution of the detected γ-rays, and $\varepsilon(E_\gamma)$ is the γ-ray detection efficiency at a transition energy E_γ. In this analysis, both 953.8(1)- and 1232.2(1)-keV γ-ray transitions are assumed to be stretched $E2$ transitions with nearly identical angular distributions $\omega(\theta)$. The parameter b_{ki} takes into account the branching ratios of all feeding transitions. To ensure a reliable extraction of the lifetime τ_i, the RDDS measurement must be carried out within a distance range in which the derivative $\frac{d}{dx} I_i^S \gtrsim \frac{1}{2}\max(\frac{dI_i^S}{dx})$ [26]. This range is called a region of sensitivity.

The relative intensity observed for the 1232.2(1)-keV transition was 80(1)% compared to the intensity of the 953.8(1)-keV transition. No other feeding transitions to the 2^+ state in ^{62}Zn were observed in these data which would allow further feeding corrections. Therefore, the DDCM analysis was carried out with two side-feeding assumptions, i.e., b_{ki} = 0.8 and 1.0. The former value equals to the assumption that the unobserved feeding to the 2_1^+ state is fast compared to the observed one. The latter value means that the unobserved side feeding has a similar time behavior to the observed one. To address ambiguity related to side-feeding effects, a $\gamma-\gamma$ coincidence analysis method can be used, as outlined in Ref. [43] (Fig. 5). In this method, the effects of side feeding in the DDCM analysis can be eliminated. In the present work, the intensities of $2_1^+ \rightarrow 0_{gs}^+$ transition in coincidence with $4_1^+ \rightarrow 2_1^+$ transition in ^{62}Zn were also analyzed as demonstrated in Fig. 6. The obtained intensities for both transitions were then analyzed in a similar fashion to the γ-ray singles analysis with the NAPATAU software (Table 2).

The lifetime values for the 2_1^+ state in ^{62}Zn were extracted at distances of 65 μm, 105 μm, 126 μm, and 156 μm, all of which lie within the region of sensitivity as can be inferred from Figs. 7 and 8. The derivatives $\frac{d}{dx} I^S_{2^+\rightarrow 0^+}$ (Figs. 7c and 8c) were obtained by fitting the $I^S_{2^+\rightarrow 0^+}$ data points (Figs. 7b and 8b) with three or two connected second-order polynomials for the Ring 1 and Ring 2 detector data, respectively. The results obtained from the γ-ray singles and $\gamma-\gamma$ coincidence analysis, summarized in Table 3, are in agreement within the uncertainties, when assuming $b_{ki} = 0.8$. This suggests that the unobserved side feeding in the γ-ray singles analysis indeed originates from shorter-lived states in comparison to the main feeding path of the 2_1^+ state validating the use of the b_{ki} value of 0.8.

The lifetime values extracted from Ring 2 appear to be systematically higher than those obtained from Ring 1, as can be seen in Table 3. The reason for this may be related to the limited number of measured distances and to the statistical variation of the individual measurement points. The fits of the polynomials shown, e.g., in Fig. 7 panels c) and d) proved to be somewhat sensitive to the selected fitting range.

4.2 MARA transmission efficiency and mass resolution

The MARA transmission efficiency is the ratio of the fusion-evaporation reaction products with specific A and Z, which pass through the separator to the focal plane, to the total number of corresponding nuclei created in the target. The transmission efficiency of a separator is an essential parameter when extracting reaction cross sections from the measurement data or alternatively when estimating the required beam time for recoil-gating or recoil-decay tagging experiments employing recoil separators [35]. A larger transmission efficiency allows a correspondingly greater yield in γ-ray statistics in these types of experiments. The most important fac-

Table 2 Fitted centroids (E_γ^S and E_γ^d) and standard deviations (σ^S and σ^d) for the fully Doppler-shifted (S) and degraded (d) components of the γ-ray peaks corresponding to the $2_1^+ \rightarrow 0_{gs}^+$ and $4_1^+ \rightarrow 2_1^+$ transitions in ^{62}Zn. The quoted values are obtained at the maximum distance of 303 μm (S) and at the minimum distance of 15 μm (d). All values are given in keV

Transition	E_γ^d	σ^d	E_γ^S	σ^S
Singles spectra				
Ring 1				
$2_1^+ \rightarrow 0_{gs}^+$	963.6(2)	2.3(2)	953.4(2)	2.3(2)
$4_1^+ \rightarrow 2_1^+$	1244.8(2)	2.4(2)	1231.8(2)	2.3(2)
Ring 2				
$2_1^+ \rightarrow 0_{gs}^+$	960.9(2)	2.2(2)	953.8(3)	2.4(2)
$4_1^+ \rightarrow 2_1^+$	1241.3(2)	2.5(2)	1231.2(2)	2.8(2)
γ–γ coincidence				
Ring 1				
$2_1^+ \rightarrow 0_{gs}^+$	960.7(4)	2.8(3)	954.3(3)	3.0(3)
$4_1^+ \rightarrow 2_1^+$	1245.8(6)	2.9(6)	1232.5(8)	3.4(7)
Ring 2				
$2_1^+ \rightarrow 0_{gs}^+$	961.4(2)	3.0(3)	954.1(2)	3.0(3)
$4_1^+ \rightarrow 2_1^+$	1242.3(4)	3.6(4)	1233.2(3)	3.9(3)

Table 3 Extracted lifetimes τ (ps) for the 2_1^+ state in ^{62}Zn obtained in the present work

	singles ($b_{ki} = 1$)		singles ($b_{ki} = 0.8$)		γ–γ	
x (μm)	Ring 1	Ring 2	Ring 1	Ring 2	Ring 1	Ring 2
65	1.1(6)	1.9(7)	3.6(6)	4.6(6)	3.1(11)	4.1(9)
105	1.0(9)	1.7(7)	3.3(7)	4.2(6)	3.5(12)	4.1(9)
126	$1.0^{+1.7}_{-1.0}$	1.8(8)	3.5(10)	4.2(7)	3.7(13)	4.1(9)
156	$1.6^{+1.9}_{-1.6}$	1.8(7)	3.9(10)	3.9(6)	3.5(15)	3.8(10)
$\tau_{\text{w.avg}}$	**1.1(5)**	**1.8(4)**	**3.6(4)**	**4.2(3)**	**3.4(7)**	**4.0(5)**

tors that affect the separator transmission efficiency are *i*) the reaction kinematics (normal, symmetric, or inverse kinematics) and employed beam energy, *ii*) the thickness of the target and degrader thickness, and *iii*) the characteristics of the separator, such as angular and energy acceptances. For example, the inverse kinematic reaction ($A_{\text{target}} < A_{\text{beam}}$), as used in the present work, typically results in higher transmission efficiency than the normal kinematic reaction ($A_{\text{target}} > A_{\text{beam}}$), while a thicker target foil results in broader angular cone, energy, and charge-state distributions of the reaction products, leading to a reduced number of recoils entering and passing through the separator. Similarly, the addition of the degrader foil increases the energy spread and broadens the angular cone of the produced nuclei, both reducing the transmission efficiency.

The MARA transmission efficiency was determined experimentally for the ^{24}Mg(^{40}Ca, 2p)^{62}Zn reaction used in the APPA commissioning experiment. This was done by taking the ratio between the number of $2_1^+ \rightarrow 0_{gs}^+$ γ rays observed in the recoil-gated (no mass gating) singles and raw JUROGAM 3 γ-ray spectra. Secondly, similar analysis was done for the number of the $4_1^+ \rightarrow 2_1^+$ γ-ray transitions in coincidence with the $2_1^+ \rightarrow 0_{gs}^+$ transitions. The recoil gating was performed separately with the DSSD and MWPC detectors. This was done because the MWPC detector has larger physical size, hence, the transmission measured at this detector position should yield a higher value. The transmission efficiency was extracted from data obtained with the $^{\text{nat}}$Mg target alone and from the data where the ^{93}Nb degrader foil was placed downstream from the target. This allowed to quantify the reduction in transmission efficiency caused by the degrader. The experimental transmission efficiencies, as extracted from the DSSD and MWPC detectors, along with the simulated transmission values [35,44,45], are summarized in Table 4.

The absolute transmission efficiency for the two-proton evaporation channel (^{62}Zn) without the degrader foil was found to be on average 23.5(4)% at MWPC and 10.5(2)% at DSSD, including all observed charge states at these detector positions. The value measured at MWPC is well in line

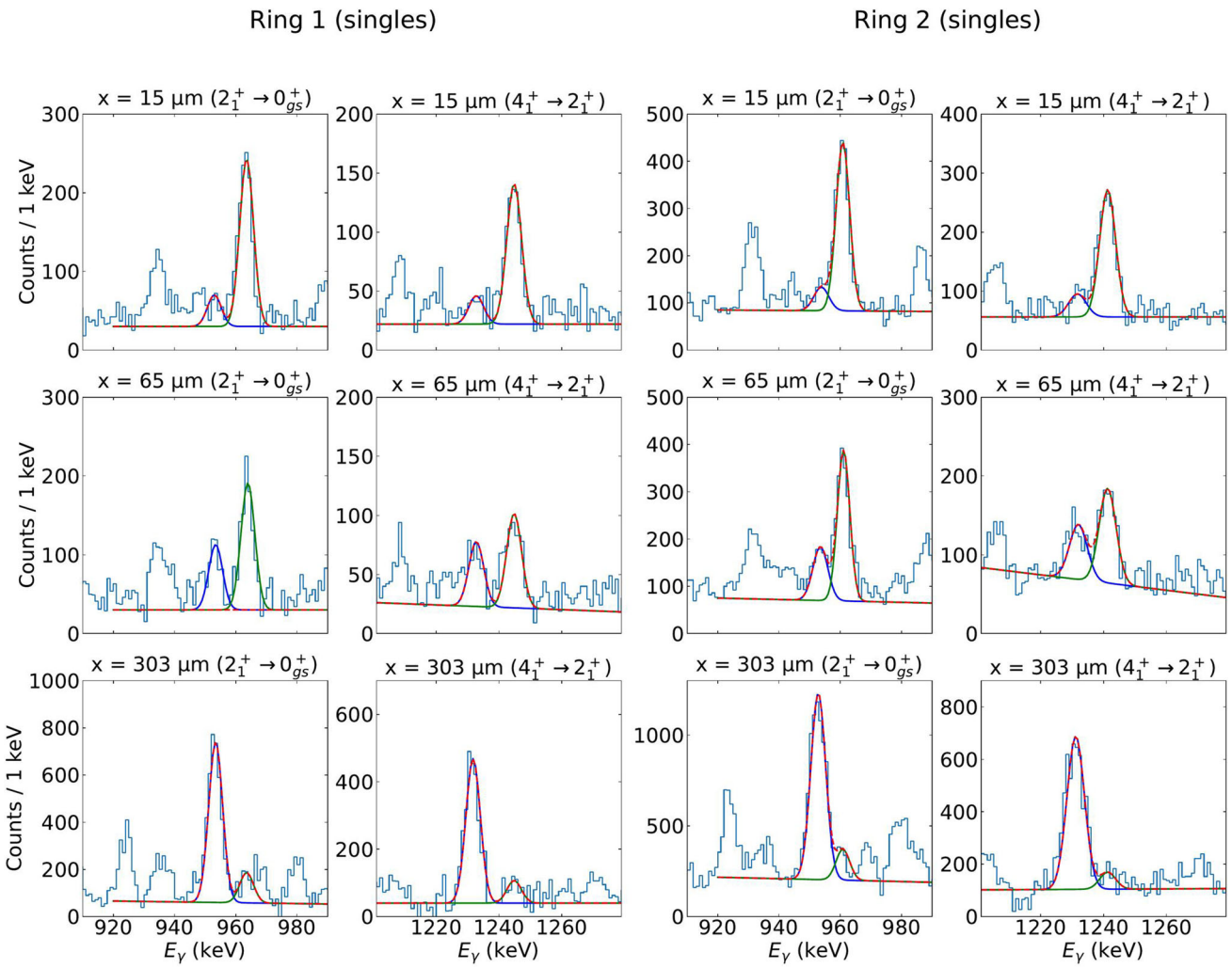

Fig. 5 Fitted γ-ray peaks in the singles analysis (employing both recoil and mass gating) corresponding to the transitions de-exciting and feeding the 2_1^+ state in ^{62}Zn from the measurements performed at distances of 15 µm, 65 µm and 303 µm. In each panel, the blue step histogram represents the measurement data. Since the spectra are Doppler corrected for the fully Doppler-shifted components, the higher-energy peaks correspond to the degraded components (green solid line), while the lower-energy peaks correspond to the fully Doppler-shifted components (solid blue line). The red solid line represents the total fit

with the transmission efficiency obtained from the ion-optical simulation as indicated in Table 4. The experimental transmission value obtained at DSSD (10.5(2)%) is somewhat lower in comparison to the simulation (14.3%), the likely reason being that the DSSD detector did not record the high-energy part of the recoil distribution, as those exceeded the set dynamic range of the DSSD preamplifiers. With the 1.33-mg/cm^2 thick ^{93}Nb degrader foil the MARA transmission efficiency was found to be reduced to average values of 10.6(3)% at MWPC and 6.1(2)% at DSSD, both being compatible with the simulated values. It should be emphasized that selecting the degrader foil material and thickness is always a compromise. A thicker foil increases the energy difference of the fully Doppler-shifted and degraded components of the γ-ray peak. On the other hand, it reduces the separator transmission efficiency and therefore γ-ray statistics in addition to potentially worsening the A/q resolution.

The MARA separator can be used to separate reaction products based on their mass-to-charge (A/q) ratios. A physical mass-slit system of MARA allows to reduce contamination, e.g., in recoil-gated or recoil-decay tagged γ-ray spectra, originating from unwanted reaction products. This is particularly important in cases where the production cross section of the nucleus of interest is low in comparison to other reaction products. Figure 9 panel a) shows the A/q distributions measured at the MARA focal plane for reaction products with masses of A = 60, 61, and 62 while using the $^{\text{nat}}$Mg target alone. It should be noted that the A/q distributions have been obtained directly from the MWPC x-position information and, hence, do not include corrections for the

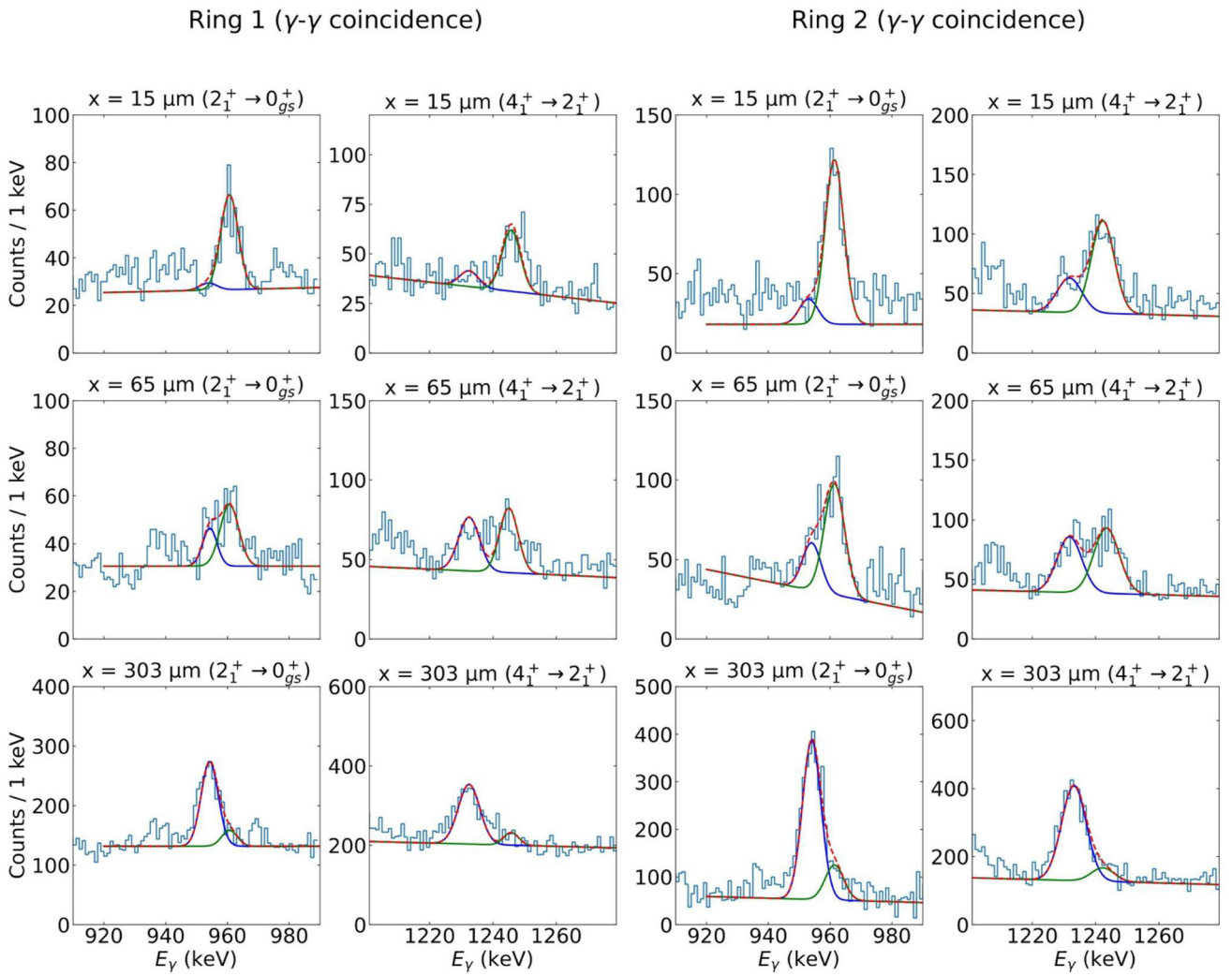

Fig. 6 Fitted γ-ray peaks in the $\gamma - \gamma$ coincidence analysis (employing stand-alone raw JUROGAM 3 data) corresponding the de-exciting transition $2_1^+ \rightarrow 0_{gs}^+$ gated with the feeding transition $4_1^+ \rightarrow 2_1^+$ in ^{62}Zn, and vice versa, from the measurements performed at distances of 15 μm, 65 μm and 303 μm. In each panel, the blue step histogram represents the measurement data. Since the spectra are Doppler corrected for the fully Doppler-shifted components, the higher-energy peaks correspond to the degraded components (green solid line), while the lower-energy peaks correspond to the fully Doppler-shifted components (solid blue line). The red solid line represents the total fit

Table 4 Experimental and simulated MARA transmission efficiencies at the DSSD and MWPC detector positions with and without the plunger degrader foil

	without degrader		with degrader	
	DSSD	MWPC	DSSD	MWPC
γ-ray singles	10.5(2)%	23.5(4)%	6.1(2)%	10.7(3)%
$\gamma - \gamma$ coincidence	9(2)%	21(3)%	5.4(12)%	8(2)%
simulation	14.3%	23.9%	6.1%	8.9%

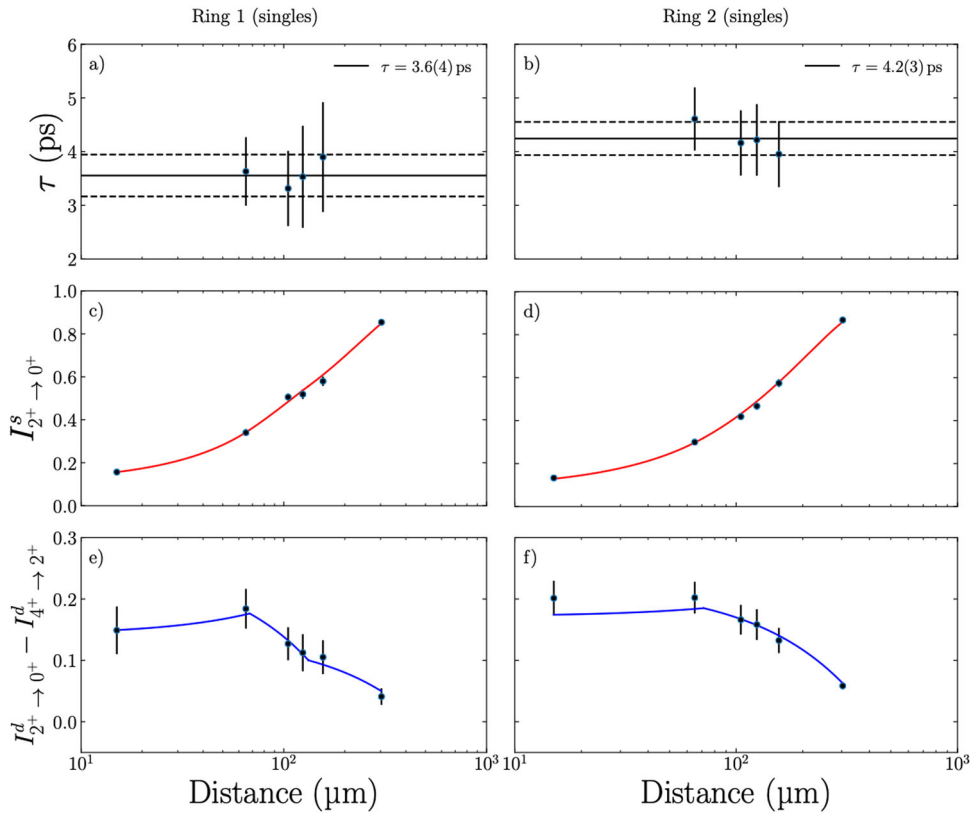

Fig. 7 Illustration of the singles lifetime analysis for the 2^+_1 state in ^{62}Zn assuming b_{ki}=0.8: **a** and **b** extracted lifetime values at distances of 65 µm, 105 µm, 126 µm, and 156 µm, with the weighted average (solid lines) and 1σ error margins (dashed lines), **c** and **d** fit of the fully Doppler-shifted normalized intensities for the $2^+_1 \to 0^+_{gs}$ transition in ^{62}Zn, and **e** and **f** the difference of the degraded normalized intensities between the de-exciting and feeding transitions of the 2^+_1 state. From left to right, the results are presented separately for Ring 1 and Ring 2

energy or angular aberrations. As the use of the degrader foil introduces both energy and angular straggling of the reaction products entering MARA, this may also affect the MARA mass resolution ($\Delta A = q \cdot w_{A/q}$) and mass-resolving power ($R = \frac{A/q}{w_{A/q}} = A/\Delta A$), where $w_{A/q}$ is the full width at half maximum (FWHM) of the A/q distribution. Panel b) in Fig. 9 shows the A/q distributions with the 1.33-mg/cm^2 thick ^{93}Nb degrader foil: As can be seen, the reaction products with neighboring masses are still well separated for the central charge states of q = 13 and q = 14. The average mass resolution without degrader for the central charge states q = 17 and q = 18 is ΔA = 0.98(6) amu translating to the mass-resolving power of R = 63.0(41). With degrader the corresponding values appear to be only marginally worse yielding ΔA = 1.00(8) amu and R = 62.8(56). In fact, the obtained mass-resolving power values in both cases are worse than the typical value of $R \sim 150$ [44]. This is most likely due to the fact that one of the ion-optical components, the surface coils of the MARA magnetic dipole were out of order during this test experiment.

4.3 The prompt γ-ray detection efficiency

The detection efficiency of prompt γ-rays from the target was determined for Rings 1 and 2 of JUROGAM 3 by using ^{152}Eu and ^{133}Ba calibration sources in four different configurations. These were *i*) a standard JUROGAM 3 configuration, *ii*) the APPA plunger without the JYUTUBE configuration, *iii*) the full APPA configuration (the plunger and JYUTUBE) and *iv*) JYUTUBE without the APPA plunger configuration. The results are shown in Fig. 10. The γ-ray detection efficiencies have been scaled so that the efficiency at 1.3 MeV in configuration 1 is 0.4% in Ring 1 and 0.9% in Ring 2 (∼0.1% / Ge detector). These absolute efficiencies are known from several previous detection efficiency measurements of JUROGAM 3. According to the results (see Fig. 10), the effect of the APPA plunger on the γ-ray detection efficiency is negligible. The γ-ray detection efficiency appears to be actually higher with the plunger, especially in the turnover region around 120 keV. This somewhat unexpected result may be attributed to slight differences in the positions of the calibration sources between the measurements. In the measurements corresponding to "standard con-

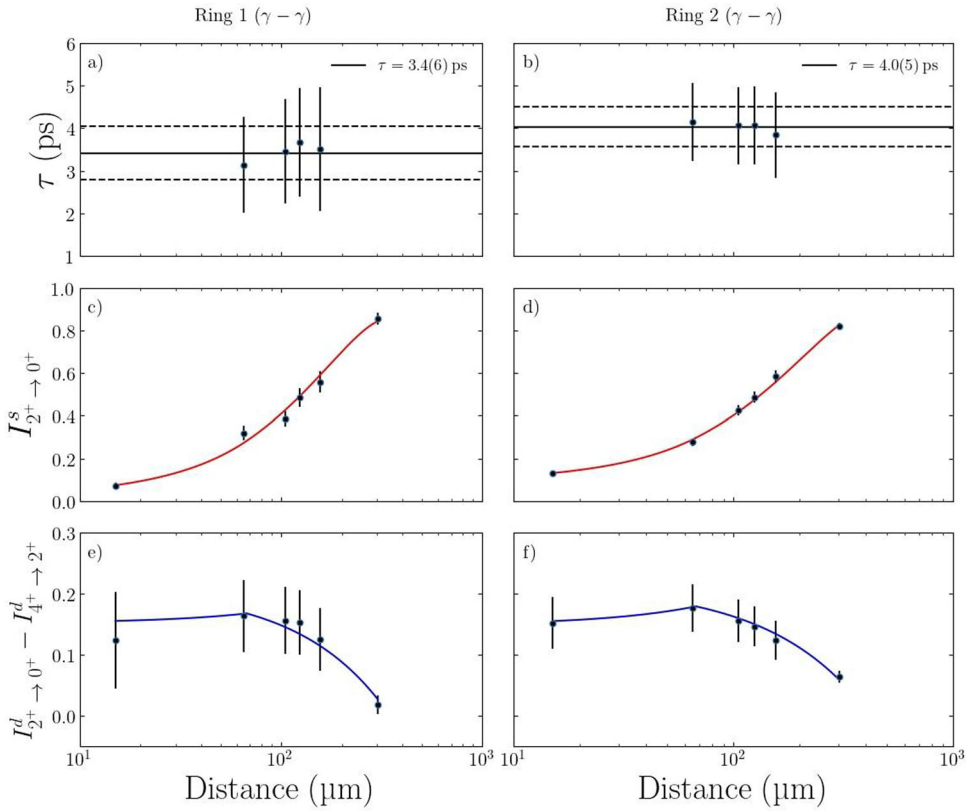

Fig. 8 The figure illustrates the $\gamma-\gamma$ coincidence lifetime analysis for the 2_1^+ state in ^{62}Zn: **a** and **b** extracted lifetime values at distances of 65 µm, 105 µm, 126 µm, and 156 µm, with the weighted average (solid lines) and 1σ error margins (dashed lines), **c** and **d** fit of the fully Doppler-shifted normalized intensities for the $2_1^+ \to 0_{gs}^+$ transition in ^{62}Zn, and **e** and **f** the difference of the degraded normalized intensities between the de-exciting and feeding transitions of the 2_1^+ state. The results are presented separately for Ring 1 and Ring 2

figuration" and "NO plunger and JYUTUBE", the calibration sources might have been at most 5 mm off the actual target position toward MARA. The addition of JYUTUBE clearly reduces the γ-ray detection efficiency. However, in many cases, JYUTUBE can provide a cleaner prompt γ-ray spectrum, which is more beneficial despite the moderate reduction in the γ-ray detection efficiency.

4.4 JYUTUBE charged-particle detection efficiency with the APPA plunger

The JYUTUBE charged-particle detection efficiency in the APPA configuration was determined by measuring the intensities of the selected recoil-gated prompt γ rays originating from the reaction products ^{61}Cu (produced in the $3p$ evaporation channel), ^{61}Zn ($2pn$), and ^{62}Zn ($2p$) as a function of the JYUTUBE charged-particle count. This approach works because the γ rays are associated with recoil events, and each recoil event is in turn associated with 0 to N detected charged-particle events in JYUTUBE. The resulting experimental distributions shown in Fig. 11 were fitted with binomial distributions, yielding an average detection efficiency of 40.2(3)% for one evaporated proton. This value is lower than the typical one-proton detection efficiency of JYUTUBE in the standard target holder configuration, where detection efficiency values of 60–70% are commonly observed. The reduction is due to the target/degrader cones and support rings of the APPA plunger, which mask the JYUTUBE detector elements located around $\theta \approx 90°$ with respect to the beam axis. The 40.2(3)% one-proton detection efficiency corresponds to a veto efficiency of about 80% for a $3p$ channel, demonstrating the usefulness of the device when measuring lifetimes in nuclei produced via xn, pxn, or αxn channels.

5 Conclusions

The performance of the APPA device has been assessed in an in-beam commissioning experiment in conjunction with the JUROGAM 3 spectrometer and the MARA separator. The lifetime of the 2_1^+ state in ^{62}Zn was measured yielding a weighted average value of $\tau = 3.9(2)$ ps based on the four individual lifetime values listed in Table 3. The value obtained is consistent with the literature value of 4.2(2) ps

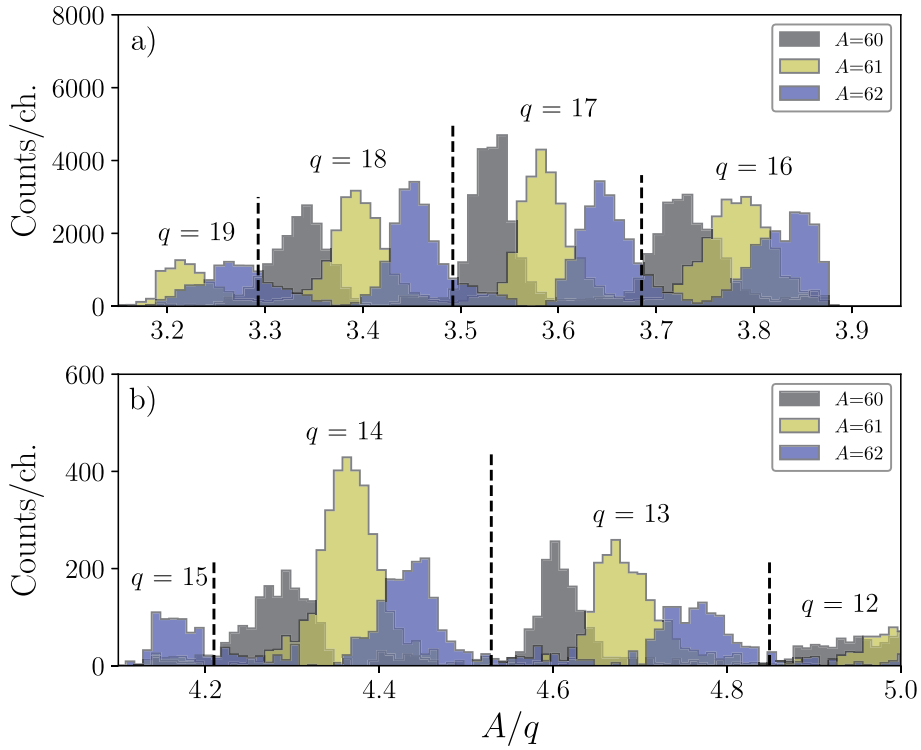

Fig. 9 The experimental mass-to-charge (A/q) distributions as measured at the MARA focal plane for reaction products with mass A = 60 (black), A = 61 (yellow) and A = 62 (blue) a) with a 0.74-mg/cm^2 thick ^{nat}Mg target foil only and b) with 0.74-mg/cm^2 thick ^{nat}Mg target and 1.33-mg/cm^2 thick ^{93}Nb degrader foils. The (A/q) distributions are formed by gating on the known prompt γ-ray transitions from ^{60}Ni, ^{61}Cu, and ^{62}Zn

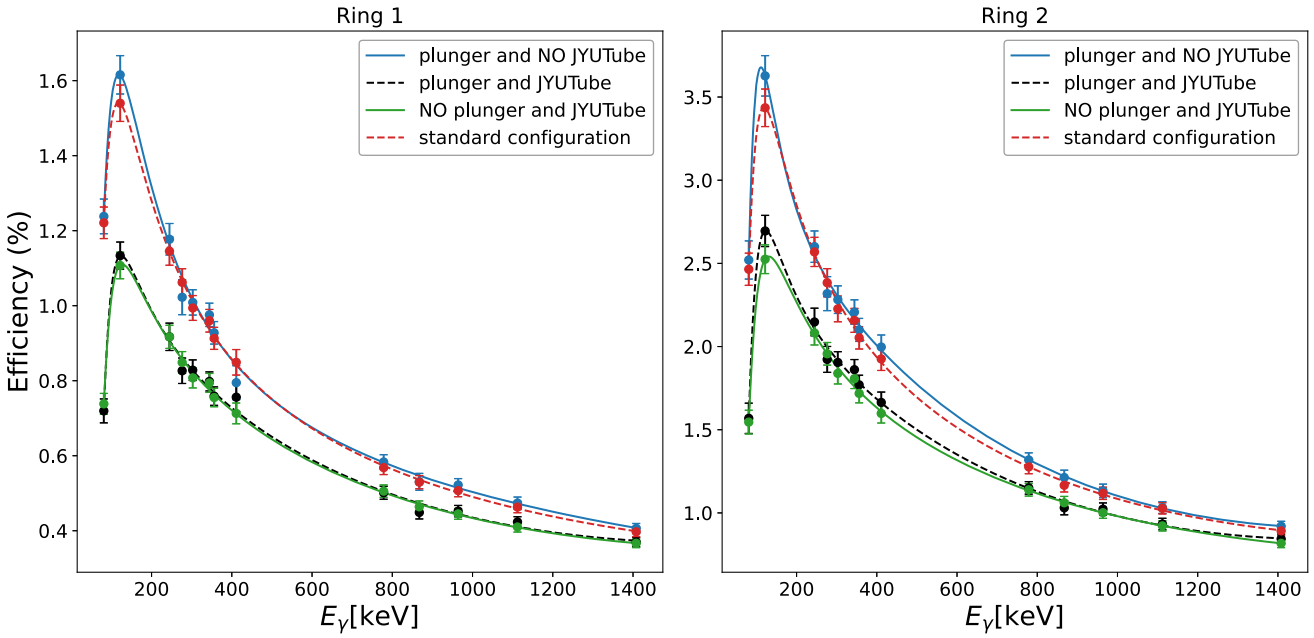

Fig. 10 The γ-ray detection efficiency curves for Ring 1 and Ring 2 of JUROGAM 3 in four different configurations: *i*) the APPA plunger without the JYUTUBE configuration (solid blue line), *ii*) the plunger and JYUTUBE (dashed red line) *iii*) the standard JUROGAM 3 configuration without JYUTUBE (solid green line) and *iv*) the standard JUROGAM 3 configuration with JYUTUBE (dashed black line)

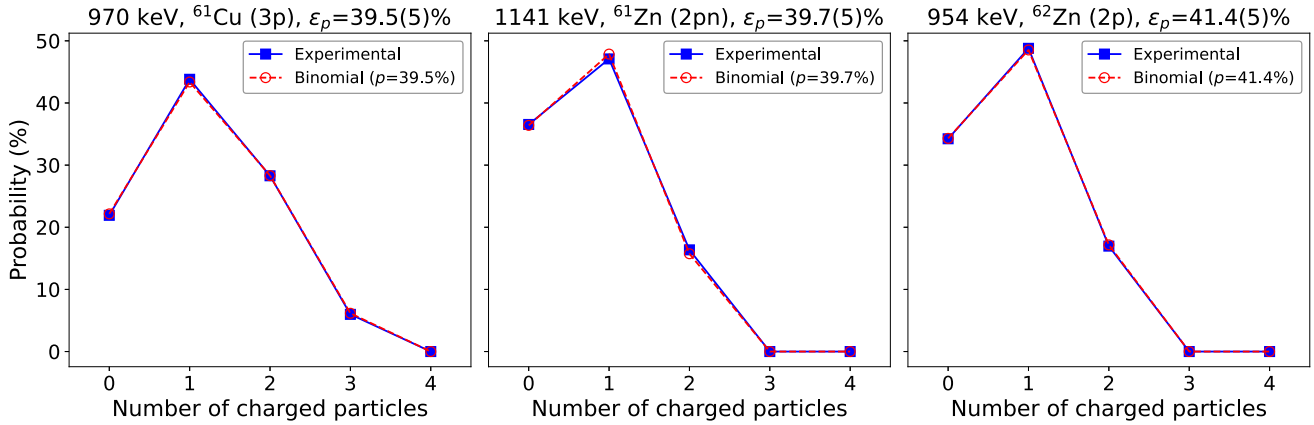

Fig. 11 Determination of the JYUTUBE detection efficiency for one evaporated proton. The experimental distributions (blue solid squares) are obtained by measuring the intensities of selected γ-rays originating from ^{61}Cu $(3p)$, ^{61}Zn $(2pn)$ and ^{62}Zn $(2p)$ nuclei as a function of the detected charged-particle count. Binomial distribution (red open symbols) is then fitted to the experimental data yielding the one-proton detection efficiencies (ϵ_p) in each case

[38]. This result validates APPA and its operational procedures in RDDS measurements with recoil separators.

Furthermore, the MARA transmission efficiency values of 10.5(2)% at DSSD and 23.5(4)% at MWPC locations were measured for the ^{62}Zn recoils from the ^{24}Mg (^{40}Ca, 2p)^{62}Zn reaction using a 0.74-mg/cm^2 thick ^{nat}Mg target. After adding the 1.33-mg/cm^2 thick ^{93}Nb plunger degrader foil, the corresponding transmission efficiency values were reduced to 6.1(2)% at DSSD and 10.6(3)% at MWPC. Moreover, the mass resolution and mass-resolving power of MARA were determined without and with the degrader foil. No significant reduction in these values was observed when the degrader foil was used. These results provide an experimental benchmark for simulations of the MARA ion-optics and facilitate better planning of the future APPA experiments at MARA. Lastly, the JYUTUBE charged-particle detection efficiency for one evaporated proton was measured to be 40.2(3)% in the APPA configuration.

Since the commissioning experiment reported in this work, the APPA device has been successfully used in several RDDS measurements employing both the RITU and MARA separators. Although most of these data are currently under analysis, three published research works reported in Refs. [4,46,47] demonstrate the excellent functionality of APPA.

Acknowledgements The authors acknowledge the GAMMAPOOL European Spectroscopy Resource for the loan of the Germanium detectors. The authors express their gratitude to the technical staff of the Accelerator Laboratory at the University of Jyväskylä for their support. Especially, J. Jaatinen is acknowledged for preparing high-quality plunger foils. CMG was supported by the U.S. Department of Energy, Office of Nuclear Physics, under the award DE-AC02-Q6CH11357. This work was also supported by the German Research Foundation (Deutsche Forschungsgemeinschaft, DFG), grant No. FR 3276/3-1.

Funding Open Access funding provided by University of Jyväskylä (JYU).

Data Availability Statement Data will be made available on reasonable request. [Authors' comment: The datasets generated during and/or analysed during the current study are available from the corresponding author on reasonable request.].

Code Availability Statement This manuscript has no associated code/software. [Authors' comment: The code/software generated during and/or analysed during the current study is available from the corresponding author on reasonable request.].

References

1. K. Kaneko, M. Hasegawa, T. Mizusaki, Shape transition and oblate-prolate coexistence in $N = Z$ fpg-shell nuclei. Phys. Rev. C **70**, 051301 (2004). https://doi.org/10.1103/PhysRevC.70.051301
2. K. Wimmer, W. Korten, P. Doornenbal, T. Arici, P. Aguilera, A. Algora, T. Ando, H. Baba, B. Blank, A. Boso, S. Chen, A. Corsi, P. Davies, G. de Angelis, G. de France, J.-P. Delaroche, D.T. Doherty, J. Gerl, R. Gernhäuser, M. Girod, D. Jenkins, S. Koyama, T. Motobayashi, S. Nagamine, M. Niikura, A. Obertelli, J. Libert, D. Lubos, T.R. Rodríguez, B. Rubio, E. Sahin, T.Y. Saito, H. Sakurai, L. Sinclair, D. Steppenbeck, R. Taniuchi, R. Wadsworth, M. Zielinska, Shape Changes in the Mirror Nuclei ^{70}Kr and ^{70}Se Phys. Rev.

Lett. **126**, 072501 (2021). https://doi.org/10.1103/PhysRevLett.126.072501
3. R.D.O. Llewellyn, M.A. Bentley, R. Wadsworth, H. Iwasaki, J. Dobaczewski, G. de Angelis, J. Ash, D. Bazin, P.C. Bender, B. Cederwall, B.P. Crider, M. Doncel, R. Elder, B. Elman, A. Gade, M. Grinder, T. Haylett, D.G. Jenkins, I.Y. Lee, B. Longfellow, E. Lunderberg, T. Mijatović, S.A. Milne, D. Muir, A. Pastore, D. Rhodes, D. Weisshaar, Establishing the Maximum Collectivity in Highly Deformed $N = Z$ Nuclei Phys. Rev. Lett. **124**, 152501 (2020). https://doi.org/10.1103/PhysRevLett.124.152501
4. A.M. Plaza, J. Pakarinen, P. Papadakis, R.D. Herzberg, J. Julin, T.R. Rodríguez, A.D. Briscoe, A. Illana, J. Ojala, P. Ruotsalainen, E. Uusikylä, B. Alayed, A. Alharbi, O. Alonso-Sañudo, K. Auranen, V. Bogdanoff. J. Chadderton, A. Esmaylzadeh, C. Fransen, T. Grahn, P.T. Greenlees, J. Jolie, J. Joukainen, H. Jutila, G.L. Zimba, Direct measurement of three different deformations near the ground state in an atomic nucleus Commun. Phys. **8**, 3659 (2025). https://doi.org/10.1038/s42005-024-01928-8
5. P.E. Garrett, M. Zielińska, E. Clément, An experimental view on shape coexistence in nuclei. Prog. Part. Nucl. Phys. **124**, 103931 (2022). https://doi.org/10.1016/j.ppnp.2021.103931
6. K. Heyde, J.L. Wood, Shape coexistence in atomic nuclei. Rev. Mod. Phys. **83**, 1467–1521 (2011). https://doi.org/10.1103/RevModPhys.83.1467 Export Citation
7. K. Heyde, J.L. Wood, Shape Coexistence in Light Se Isotopes: Evidence for Oblate Shapes, Phys. Rev. Lett. **100**, 1467–1521, 102502 (2008). https://doi.org/10.1103/PhysRevLett.100.102502
8. A.Z. Schwarzschild, E.K. Warburton, The Measurement of Short Nuclear Lifetimes Annu. Rev. Nucl. Part. Sci. **18**, 265–290 (1968). https://doi.org/10.1146/annurev.ns.18.120168.001405
9. A.F. Lisetskiy, N. Pietralla, M. Honma, A. Schmidt, I. Schneider, A. Gade, P. von Brentano, T. Otsuka, T. Mizusaki, B.A. Brown, Experimental evidence for ^{56}Ni-core breaking from the low-spin structure of the $N = Z$ nucleus ^{58}Cu Phys. Rev. C **68**, 034316 (2003). https://doi.org/10.1103/PhysRevC.68.034316
10. A.J. Nichols, R. Wadsworth, H. Iwasaki, K. Kaneko, A. Lemasson, G. de Angelis, V.M. Bader, T. Baugher, D. Bazin, M.A. Bentley, J.S. Berryman, T. Braunroth, P.J. Davies, A. Dewald, C. Fransen, A. Gade, M. Hackstein, J. Henderson, D.G. Jenkins, D. Miller, C. Morse, I. Paterson, E.C. Simpson, S.R. Stroberg, D. Weisshaar, K. Whitmore, K. Wimmer, Collectivity in A∼70 nuclei studied via lifetime measurements in ^{70}Br and ^{68,70}Se Phys. Lett. B **733**, 52–57 (2014). https://doi.org/10.1016/j.physletb.2014.04.016
11. C. Morse, H. Iwasaki, A. Lemasson, A. Dewald, T. Braunroth, V.M. Bader, T. Baugher, D. Bazin, J.S. Berryman, C.M. Campbell, A. Gade, C. Langer, I.Y. Lee, C. Loelius, E. Lunderberg, F. Recchia, D. Smalley, S.R. Stroberg, R. Wadsworth, C. Walz, D. Weisshaar, A. Westerberg, K. Whitmore, K. Wimmer, Lifetime measurement of the 2_1^+ state in ^{74}Rb and isospin properties of quadrupole transition strengths at $N = Z$ Phys. Lett. B **787**, 198–203 (2018). https://doi.org/10.1016/j.physletb.2018.10.064
12. O. Möller et al., Transition probabilities and isospin structure in the $N = Z$ nucleus ^{46}V Phys. Rev. C **67**, 011301 (2003). https://doi.org/10.1103/PhysRevC.67.011301
13. A. Boso, S.A. Milne, M.A. Bentley, F. Recchia, S.M. Lenzi, D. Rudolph, M. Labiche, X. Pereira-Lopez, S. Afara, F. Ameil, T. Arici, S. Aydin, M. Axiotis, D. Barrientos, G. Benzoni, B. Birkenbach, A.J. Boston, H.C. Boston, P. Boutachkov, A. Bracco, A.M. Bruce, B. Bruyneel, B. Cederwall, E. Clement, M.L. Cortes, D.M. Cullen, P. Désesquelles, Zs. Dombràdi, C. Domingo-Pardo, J. Eberth, C. Fahlander, M. Gelain, V. González, P.R. John, J. Gerl, P. Golubev, M. Górska, A. Gottardo, T. Grahn, L. Grassi, T. Habermann, L.J. Harkness-Brennan, T.W. Henry, H. Hess, I. Kojouharov, W. Korten, N. Lalović, M. Lettmann, C. Lizarazo, C. Louchart-Henning, R. Menegazzo, D. Mengoni, E. Merchan, C. Michelagnoli, B. Million, V. Modamio, T. Moeller, D.R. Napoli, J. Nyberg, B.S. Nara Singh, H. and Pai, N. Pietralla, S. Pietri, Zs. Podolyak, R.M. Perez Vidal, A. Pullia, D. Ralet, G. Rainovski, M. Reese, P. Reiter, M.D. Salsac, E. Sanchis, L.G. Sarmiento, H. Schaffner, L.M. Scruton, P.P. Singh, C. Stahl, S. Uthayakumaar, J.J. Valiente-Dobón, O. Wieland, Isospin dependence of electromagnetic transition strengths among an isobaric triplet Phys. Lett. B **797**, 134835 (2019). https://doi.org/10.1016/j.physletb.2019.134835
14. M.M. Giles, B.S. Nara Singh, L. Barber, D.M. Cullen, M.J. Mallaburn, M. Beckers, A. Blazhev, T. Braunroth, A. Dewald, C. Fransen, A. Goldkuhle, J. Jolie, F. Mammes, C. Müller-Gatermann, D. Wölk, K.O. Zell, S.M. Lenzi, A. Poves, Probing isospin symmetry in the (^{50}Fe, ^{50}Mn, ^{50}Cr) isobaric triplet via electromagnetic transition rates Phys. Rev. C **99**, 044317 (2019). https://doi.org/10.1103/PhysRevC.99.044317
15. A.N. Steer, D.G. Jenkins, R. Glover, B.S. Nara Singh, N.S. Pattabiraman, R. Wadsworth, S. Eeckhaudt, T. Grahn, P.T. Greenlees, P. Jones, R. Julin, S. Juutinen, M. Leino, M. Nyman, J. Pakarinen, P. Rahkila, J. Sarén, C. Scholey, J. Sorri, J. Uusitalo, P.A. Butler, I.G. Darby, R.-D. Herzberg, D.T. Joss, R.D. Page, J. Thomson, R. Lemmon, J. Simpson, B. Blank, Recoil-beta tagging: A novel technique for studying proton-drip-line nuclei Nucl. Instrum. Methods Phys. Res. A, **565**(2), 630–636 (2006). https://doi.org/10.1016/j.nima.2006.06.034
16. K. Wimmer, P. Ruotsalainen, S.M. Lenzi, A. Poves, T. Hüyük, F. Browne, P. Doornenbal, T. Koiwai, T. Arici, K. Auranen, M.A. Bentley, M.L. Cortés, C. Delafosse, T. Eronen, Z. Ge, T. Grahn, P.T. Greenlees, A. Illana, N. Imai, H. Joukainen, R. Julin, A. Jungclaus, H. Jutila, A. Kankainen, N. Kitamura, B. Longfellow, J. Louko, R. Lozeva, M. Luoma, B. Mauss, D.R. Napoli, M. Niikura, J. Ojala, J. Pakarinen, X. Pereira-Lopez, P. Rahkila, F. Recchia, M. Sandzelius, J. Sarén, R. Taniuchi, H. Tann, S. Uthayakumaar, J. Uusitalo, V. Vaquero, R. Wadsworth, G. Zimba, R. Yajzey, Isospin symmetry in the T = 1, A = 62 triplet Phys. Lett. B **847**, 138249 (2023). https://doi.org/10.1016/j.physletb.2023.138249
17. H. Joukainen, P. Ruotsalainen, J. Sarén, P.C. Srivastava, D. Patel, R. Julin, K. Auranen, Z. Ge, T. Grahn, P. Greenlees, A. Illana, H. Jutila, M. Leino, J. Louko, M. Luoma, J. Ojala, J. Pakarinen, P. Rahkila, M. Sandzelius, H. Tann, J. Uusitalo, G.L. Zimba, γ-Ray spectroscopy above the 9^+ isomeric state in the $N = Z$ nucleus ^{66}As Eur. Phys. J. A **60**, 241 (2024). https://doi.org/10.1140/epja/s10050-024-01458-5
18. G.L. Zimba et al., Isospin symmetry breaking in the T=1, A=70 triplet Phys. Rev. C **110**, 024314 (2024). https://doi.org/10.1103/PhysRevC.110.024314
19. G.L. Zimba et al., First Identification of Excited States in ^{78}Zr and Implications for Isospin Nonconserving Forces in Nuclei Phys. Rev. Lett. **134**, 022502 (2025). https://doi.org/10.1103/PhysRevLett.134.022502
20. P. Voss, R. Henderson, C. Andreoiu, R. Ashley, R.A.E. Austin, G.C. Ball, P.C. Bender, A. Bey, A. Cheeseman, A. Chester, D.S. Cross, T.E. Drake, A.B. Garnsworthy, G. Hackman, R. Holland, S. Ketelhut, P. Kowalski, R. Krücken, A.T. Laffoley, K.G. Leach, D. Miller, W.J. Mills, M. Moukaddam, C.J. Pearson, J. Pore, E.T. Rand, M.M. Rajabali, U. Rizwan, J. Shoults, K. Starosta, C.E. Svensson, E. Tardiff, C. Unsworth, K. Van Wieren, Z.-M. Wang, J. Williams, The TIGRESS Integrated Plunger ancillary systems for electromagnetic transition rate studies at TRIUMF Nucl. Instrum. Methods Phys. Res. A **746**, 87–97 (2014). https://doi.org/10.1016/j.nima.2014.02.006
21. C. Müller-Gatermann, F. von Spee, A. Goasduff, D. Bazzacco, M. Beckers, T. Braunroth, A. Boso, P. Cocconi, G. de Angelis, A. Dewald, C. Fransen, A. Goldkuhle, A. Gottardo, A. Gozzelino, K. Hadynska-Klek, G. Jawroski, P.R. John, J. Jolie, S.M. Lenzi, J. Litzinger, R. Menegazzo, D. Mengoni, D.R. Napoli, F. Recchia, M. Siciliano, D. Testov, S. Thiel, J.J. Valiente-Dobon, K.O. Zell,

A new dedicated plunger device for the GALILEO γ-ray detector array Nucl. Instrum. Methods Phys. Res. A **920**, 95–99 (2019). https://doi.org/10.1016/j.nima.2018.12.077
22. A. Dewald, R. Peusquens, B. Saha, P. Von Brentano, A. Fitzler, T. Klug, I. Wiedenhöver, M. Carpenter, A. Heinz, R. Janssens, F. Kondev, C. Lister, D. Seweryniak, K. Abu Saleem, R. Krücken, J., Cooper, C. Barton, K. Zyromski, C. Beausang, Z. Wang, P. Petkov, A. Oros Peusquens, U. Garg, S. and (2003). Recoil-gated plunger lifetime measurements in ^{188}Pb. Phys. Rev. C. https://doi.org/10.17615/fjv1-v314
23. F. Galtarossa, A. Gottardo, L. Zago, M. Balogh, E. Pilotto, G. Pasqualato, D. Mengoni, P. Aguilera Jorquera, G. Andreetta, F. Angelini, L. Baldesi, J. Benito, G. Benzoni, S. Bottoni, D. Brugnara, A. Camaiani, S. Carollo, J. Collado, G. Corbari, M. D'Andrea, G. De Angelis, M. Del Fabbro, D. Dell'Aquila, J. Diklić, F. Dunkel, F. Ercolano, A. Ertoprak, A. Gadea, A. Giaz, A. Goasdúff, C. Góngora-Servín, A. Gozzelino, K. Hadyńska-Klek, C. Hiver, Z. Huang, M. Kaci, H. Kleis, S.M. Lenzi, I. and Lombardo, N. Marchini, H. Mayr, R. Menegazzo, N. Miani, A. Nannini, D.R. Napoli, R. Nicolás del Álamo, J. Pellumaj, R.M. Pérez-Vidal, S. Pigliapoco, M. Polettini, F. Recchia, L. Redigolo, K. Rezynkina, M. Rocchini, M. Sedlák, A. Spacek, F. Spee, G. Spina, D. Stramaccioni, J.J. Valiente-Dobón, I. Zanon, G. Zhang, Lifetime measurement after direct transfer reactions with AGATA at LNL, EPJ Web of Conferences **324**, 00029 (2025). https://doi.org/10.1051/epjconf/202532400029
24. J. Pakarinen, J. Ojala, P. Ruotsalainen, H. Tann, H. Badran, T. Calverley, J. Hilton, T. Grahn, P.T. Greenlees, M. Hytönen, A. Illana, A. Kauppinen, M. Luoma, P. Papadakis, J. Partanen, K. Porras, M. Puskala, P. Rahkila, K. Ranttila, J. Sarén, M. Sandzelius, S. Szwec, J. Tuunanen, J. Uusitalo, G. Zimba, The JUROGAM 3 spectrometer Eur. Phys. J. A **56**, 149 (2020). https://doi.org/10.1140/epja/s10050-020-00144-6
25. Q-521 Q-Motion Miniature Linear Stage Physik Instrumente, (2025)
26. A. Dewald, O. Möller, P. Petkov, Developing the Recoil Distance Doppler-Shift technique towards a versatile tool for lifetime measurements of excited nuclear states Prog. Part. Nucl. Phys. **67**(3), 786–839 (2012). https://doi.org/10.1016/j.ppnp.2012.03.003
27. Berkeley Nucleonics Corporation, Model PB-5 Precision NIM Pulse Generator (2025)
28. National Instruments, NI USB-6212 (2025). https://www.ni.com/docs/en-US/bundle/usb-6212-specs/page/specs.html
29. M. Beckers, A. Dewald, C. Fransen, K. Arnswald, C. Müller-Gatermann, F. von Spee, Development of the multi-purpose Cologne Compact Differential Plunger (CoCoDiff) for the measurement of nuclear level lifetimes with the Recoil Distance Doppler-shift method Nucl. Instrum. Methods Phys. Res. A **1042**, 167418 (2022). https://doi.org/10.1016/j.nima.2022.167418
30. A. Dewald, S. Harissopulos, P. von Brentano, The Differential Plunger and the Differential Decay Curve Method for the Analysis of Recoil Distance Doppler-Shift Data Z. Phys. A **334**, 163–175 (1989)
31. J. Altmann, A. Dewald, K.O. Zell, P. von Brentano, Beam-induced bumps in plunger targets, a threshold effect Nucl. Instrum. Methods Phys. Res. A **321**(1), 59–63 (1992). https://doi.org/10.1016/0168-9002(92)90377-G
32. T.K. Alexander, A. Bell, A target chamber for recoil-distance lifetime measurements Nucl. Instrum. Methods Phys. Res. **81**(1), 22–26 (1970). https://doi.org/10.1016/0029-554X(70)90604-X
33. M. Beckers, A. Dewald, C. Fransen, L. Kornwebel, C.-D. Lakenbrink, F. von Spee, Revisiting the measurement of absolute foil-separation for RDDS measurements and introduction of an optical measurement method Nucl. Instrum. Methods Phys. Res. A **1042**, 167416 (2022). https://doi.org/10.1016/j.nima.2022.167416
34. E. Liukkonen, New K130 cyclotron at Jyväskylä, in: 13th International Conference on Cyclotrons, 22 (1993)
35. J. Uusitalo, J. Sarén, J. Partanen, J. Hilton, Mass Analyzing Recoil Apparatus. MARA Acta Phys. Pol. B **50**(3), 319–327 (2019). https://doi.org/10.5506/APhysPolB.50.319
36. P. Rahkila, Grain-A Java data analysis system for Total Data Readout Nucl. Instrum. Methods Phys. Res. A **595**(3), 637–642 (2008). https://doi.org/10.1016/j.nima.2008.08.039
37. B. Saha, Bestimmung der Lebensdauern kollektiver Kernanregungen in 124-Xe und Entwicklung von entsprechender Analysesoftware Ph.D. thesis, Universität zu Köln, (2004). http://kups.ub.uni-koeln.de/id/eprint/1246
38. A.L. Nichols, B. Singh, J.K. Tuli, Nuclear Data Sheets for ^{62}Zn Nucl. Data Sheets, **113**(4), 973–1114 (2012). https://www.nndc.bnl.gov/nudat3/getdataset.jsp?nucleus=62Zn&unc=NDS
39. K. Starosta, A. Dewald, A. Dunomes, P. Adrich, A.M. Amthor, T. Baumann, D. Bazin, M. Bowen, B.A. Brown, A. Chester, A. Gade, D. Galaviz, T. Glasmacher, T. Ginter, M. Hausmann, M. Horoi, J. Jolie, B. Melon, D. Miller, V. Moeller, R.P. Norris, T. Pissulla, M. Portillo, W. Rother, Y. Shimbara, A. Stolz, C. Vaman, P. Voss, D. Weisshaar, V. Zelevinsky, Shape and Structure of $N = Z$ ^{64}Ge: Electromagnetic Transition Rates from the Application of the Recoil Distance Method to a Knockout Reaction Phys. Rev. Lett. **99**, 042503 (2007). https://doi.org/10.1103/PhysRevLett.99.042503
40. O. Kenn, K.-H. Speidel, R. Ernst, S. Schielke, S. Wagner, J. Gerber, P. Maier-Komor, F. Nowacki, Measurements of g factors and lifetimes of low-lying states in $^{62-70}$Zn and their shell model implication Phys. Rev. C **65**, 034308 (2002). https://doi.org/10.1103/PhysRevC.65.03430
41. N.J. Ward, L.P. Ekstrom, G.D. Jones, F. Kearns, T.P. Morrison, O.M. Mustaffa, D.N. Simister, P.J. Twin, R. Wadsworth, Gamma-ray studies of ^{62}Zn. J. Phys. G: Nucl. Part. Phys. **7**(6), 815 (1981). https://doi.org/10.1088/0305-4616/7/6/014
42. J.F. Bruandet, Tsan Ung. Chan, C. Morand, M. Agard, A. Giorni, F. Glasser, Core-plus-particle coupling description of the ^{63}Zn high-spin levels Nucl. Phys. A, **288**, 15–34 (1977)
43. D. Ward, H.R. Andrews, J.S. Geiger, R.L. Graham, J.F. Sharpey-Schafer, Phys. Rev. Lett. **30**, 493 (1973)
44. J. Sarén, Private communication (2024)
45. D. Lazzaretto, Private communication (2025)
46. I. Zanon, M. Doncel, B. Cederwall, T. Grahn, A. Illana, G. Appagere, K. Auranen, T. Bäck, V. Bogdanoff, A.D. Briscoe, E.A. Cederlöf, G. González-Briz, P.T. Greenlees, R. Makwana, R. Jashbhai H. Joukainen, R. Julin, H. Jutila, D. Knežević, J. Luoko, M. Luoma, A. McCarter, B.S. Singh, J. Nara, J. Pakarinen, A.M. Plaza, P. Rahkila, P. Ruotsalainen, J. Sarén, C. Sullivan, P.-E. Tegnér, E.Uusikylä, J. Uusitalo, G.L. Zimba, Anomalous $B_{4/2}$ ratio in the yrast band of ^{167}Os Phys. Rev. C, **111**, 034323 (2025). https://doi.org/10.1103/PhysRevC.111.034323
47. A.M. Plaza, J. Pakarinen, R. Julin, P. Papadakis, R.-D. Herzberg, A.D. Briscoe, A. Illana, J. Ojala, P. Ruotsalainen, E. Uusikylä, B. Alayed, A. Alharbi, O. Alonso-Sañudo, K. Auranen, V. Bogdanoff, J. Chadderton, A. Esmaylzadeh, C. Fransen, T. Grahn, P.T. Greenlees, J. Jolie, H. Joukainen, H. Jutila, C. Lakenbrink, M. Leino, J. Louko, M. Luoma, A. McCarter, B.S. Nara Singh, P. Rahkila, A. Raggio, J. Romero, J. Sarén, N.-M. Satrazani, M. Stryjczyk, C.M. Sullivan, Á. Tolosa-Delgado, J. Uusitalo, F. von Spee, J. Warbinek, G.L. Zimba, Shape coexistence and particle-core coupling in 189Pb and 191Pb nuclei Phys. Lett. B, **139906**, 0370-2693 (2025). https://www.sciencedirect.com/science/article/pii/S0370269325006653